Laboratory Investigation

Stereotactic and Functional Neurosurgery

Stereotact Funct Neurosurg 2011;89:141–151
DOI: 10.1159/000323544

Received: September 18, 2010
Accepted after revision: December 10, 2010
Published online: April 14, 2011

Novel Platform for MRI-Guided Convection-Enhanced Delivery of Therapeutics: Preclinical Validation in Nonhuman Primate Brain

R. Mark Richardson[a] Adrian P. Kells[a] Alastair J. Martin[b] Paul S. Larson[a] Philip A. Starr[a] Peter G. Piferi[c] Geoffrey Bates[c] Lisa Tansey[c] Kathryn H. Rosenbluth[a] John R. Bringas[a] Mitchel S. Berger[a] Krystof S. Bankiewicz[a]

Departments of [a]Neurological Surgery and [b]Radiology, University of California San Francisco, San Francisco, Calif., and [c]SurgiVision Inc., Irvine, Calif., USA

Key Words
Convection-enhanced delivery · Interventional MRI · Gene therapy · Drug delivery

Abstract
Background/Aims: A skull-mounted aiming device and integrated software platform has been developed for MRI-guided neurological interventions. In anticipation of upcoming gene therapy clinical trials, we adapted this device for real-time convection-enhanced delivery of therapeutics via a custom-designed infusion cannula. The targeting accuracy of this delivery system and the performance of the infusion cannula were validated in nonhuman primates. ***Methods:*** Infusions of gadoteridol were delivered to multiple brain targets and the targeting error was determined for each cannula placement. Cannula performance was assessed by analyzing gadoteridol distributions and by histological analysis of tissue damage. ***Results:*** The average targeting error for all targets (n = 11) was 0.8 mm (95% CI = 0.14). For clinically relevant volumes, the distribution volume of gadoteridol increased as a linear function ($R^2 = 0.97$) of the infusion volume (average slope = 3.30, 95% CI = 0.2). No infusions in any target produced occlusion, cannula reflux or leakage from adjacent tracts, and no signs of unexpected tissue damage were observed. ***Conclusions:*** This integrated delivery platform allows real-time convection-enhanced delivery to be performed with a high level of precision, predictability and safety. This approach may improve the success rate for clinical trials involving intracerebral drug delivery by direct infusion.

Introduction

Convection-enhanced delivery (CED) of macromolecules directly into the brain parenchyma was first described by Bobo et al. [1] 16 years ago. CED is a term that denotes the use of a pressure gradient to generate bulk flow within the brain parenchyma, i.e. convection of macromolecules within the interstitial fluid driven by infusing a solution through a cannula placed directly in the targeted structure. This method allows therapeutic agents to be homogenously distributed through large volumes of brain tissue by bypassing the blood brain barrier and surpassing simple diffusion. Following the successful use of CED in preclinical studies of AAV2-AADC in Parkin-

KARGER

Fax +41 61 306 12 34
E-Mail karger@karger.ch
www.karger.com

Accessible online at:
www.karger.com/sfn

R. Mark Richardson, MD, PhD
Department of Neurological Surgery
505 Parnassus Avenue, Room M779
San Francisco, CA 94143-0112 (USA)
E-Mail richardsonma@neurosurg.ucsf.edu

sonian nonhuman primates (NHP) [2–5], CED has been used to deliver this gene therapy to Parkinson's disease patients with encouraging results in an initial phase I trial [6, 7].

To increase the translation of positive results from preclinical intracerebral drug delivery studies into successful clinical trials, we have evolved a method for real-time CED (RCD) over several years that has been modeled extensively in NHP. Visualizing infusions in real time provides the neurosurgeon with rapid feedback on the physical and anatomic diffusion parameters important for optimizing gene transfer and reduces the potential for adverse effects. Initially described by Bobo et al. [1] using albumin-linked surrogate tracers [8], our current technique of RCD employs interventional MRI (inMRI) to monitor the distribution of therapeutic agents that are coinfused with gadolinium-related tracers [9]. Our initial work with gadolinium-loaded liposomes [10, 11] has progressed to the coinfusion of free gadoteridol for predicting the distribution of protein [12] and AAV2 vectors [9, 11, 13]. A similar strategy, coinfusion of therapeutic agents and Gd-diethylenetriamene pentaacetic acid (Gd-DTPA), has been used by Lonser et al. [14] to treat patients with intrinsic brainstem lesions in clinical trials at the National Institutes of Health.

The safety and success of RCD in initial clinical use, combined with preclinical data demonstrating improved control of infusate delivery and prediction of therapeutic distribution, indicate that future clinical trials of intracerebral direct drug delivery should employ this treatment strategy. In order to further maximize the potential of this technology, a novel integrated hardware/software platform for RCD has been developed. The ClearPoint system, intended to provide prospective stereotactic guidance for the placement and operation of devices using inMRI, was modified to deliver a custom-designed, clinical CED catheter. We further adapted this device for use with NHP and report here the initial validation of the safety and accuracy of this device for RCD.

Methods

Animals

Two adult rhesus monkeys *(Macaca mulata)* were included in the study. Experiments were performed according to National Institutes of Health guidelines and to protocols approved by the Institutional Animal Care and Use Committee at the University of California San Francisco. NHPs were scanned on a Siemen's Magnetom Avanto 1.5T MRI using an array of 2 custom-built receive-only coils positioned on the left and right sides of the head. Each animal received 2 or 3 infusions of 1 mM gadoteridol (Prohance, Bracco Diagnostics) in 1 hemisphere during a first MRI session, and 2 or 3 infusions in the contralateral hemisphere during a second MRI session. NHP recovered for 2–3 weeks between infusion sessions. NHP were monitored daily over the course of the study by trained veterinary nurses.

Surgical Procedures

Infusions were performed in a research magnet shared between human and nonhuman primate use. Due to institutional regulations prohibiting procedures that expose animal blood products in such an area, the surgical placement and removal of the skull-mounted aiming device (SmartFrame; fig. 1) did not occur in the inMRI suite, as would occur in patients. Two weeks prior to infusion, NHPs underwent stereotactic placement of skull-mounted, MRI-compatible, threaded plastic adapter plugs (12 mm diameter × 14 mm height) for later attachment of the SmartFrame. After performing bilateral craniectomies, 1 plug was secured to the skull over each hemisphere with dental acrylic. After placement of the adapter plugs, the animals recovered for at least 2 weeks before initiation of inMRI infusion procedures.

ClearPoint System

The ClearPoint system consists of the SmartFrame, an infusion cannula, and a software system that communicates with both the MRI console and the operating neurosurgeon in the MRI suite. The ClearPoint software allows registration of the anterior commissure (AC) and posterior commissure (PC) from an initial MRI scan, selection of a target for cannula tip placement in AC-PC space and planning of the cannula trajectory. Although the entry point was relatively fixed in the NHP due to use of the adapter plug, in the clinical system the entry point is modifiable in the precraniotomy planning stage as the trajectory is adjusted. The SmartFrame houses an MRI-visible (gadolinium-impregnated) fluid stem and integrated fiducials, which are detected by the software (fig. 2). The fluid stem, which also serves as the infusion cannula guide, is aligned to the target trajectory via both 'pitch and roll' axes and an X-Y translational stage. This is accomplished using an attached hand controller resting at the opening of the MRI bore, according to directions generated by the software in response to serial T1 MRI sequences, until the fluid stem alignment matches the chosen target trajectory.

Trajectory Planning and Cannula Insertion

On the day of infusion, NHP were sedated with ketamine (Ketaset, 7 mg/kg, intramuscular) and xylazine (Rompun, 3 mg/kg, intramuscular), intubated and placed on inhaled isoflurane (1–3%). The plug adapter was prepared using sterile techniques and the NHP was placed in an MRI-compatible stereotactic frame in the supine position. Vital signs were monitored throughout the procedure, and an MRI-compatible anesthesia machine was used. The SmartFrame was attached by screwing the base onto the adapter plug over 1 hemisphere. The NHP was moved into the bore and a controller was attached to the SmartFrame by inserting guide wires into each of 4 adjustment knobs. This controller allows the surgeon to manually 'dial-in' distance changes to align the cannula to the desired trajectory in 4 planes (pitch, roll, anterior-posterior, medial-lateral) as instructed by the ClearPoint software.

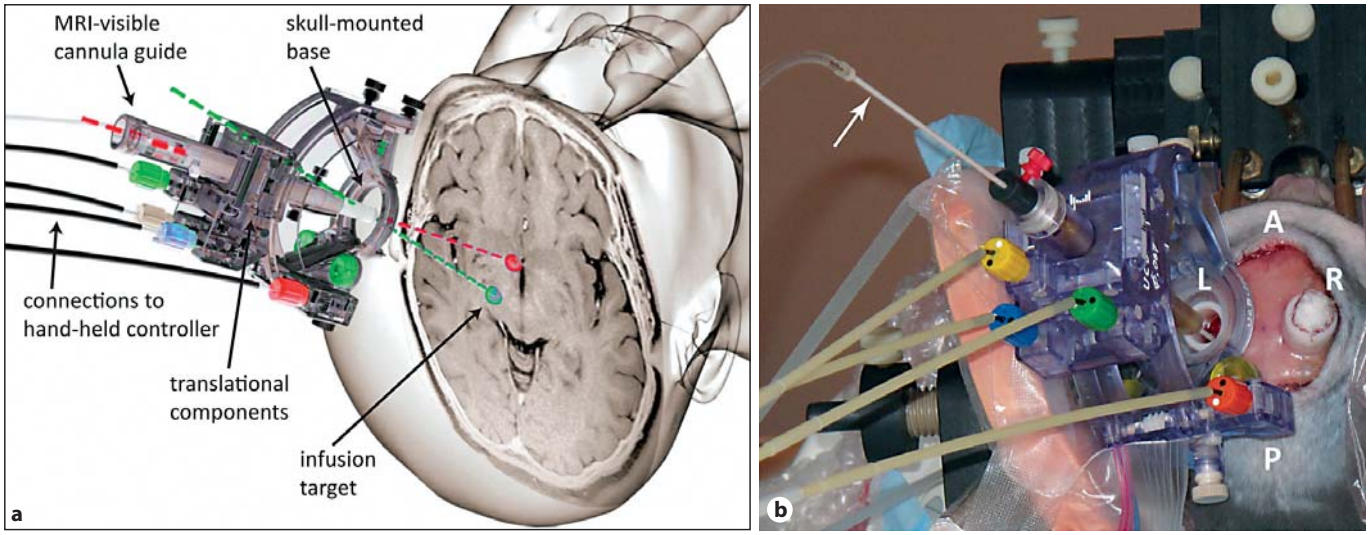

Color version available online

Fig. 1. Description of skull-mounted aiming device. **a** Basic components of the SmartFrame. **b** SmartFrame mounted on the left skull plug of a NHP, in a similar orientation to that depicted in **a**. The cannula (arrow) has been inserted through the fluid stem. A = Anterior; P = posterior; R = right; L = left.

First, a high-resolution anatomical MR scan was acquired for target identification and surgical planning. The scan was a 9-min 3D Magnetization Prepared Rapid Gradient Echo (MPRAGE) acquired with near-isotropic voxel dimensions of 0.7 × 0.7 × 1 mm over a 180-mm field of view (FOV) with 128 slices, an echo time (TE) of 3.76 ms, an inversion time (TI) of 1,100 ms, a repetition time (TR) of 2,170 ms, a 15-degree flip angle and a bandwidth of 130 Hz/pixel. The MPRAGE images were then transferred to the ClearPoint system, where the target for cannula tip placement was selected (fig. 3a). Next, rapid scans were obtained that allowed the ClearPoint software to detect the position and orientation of the SmartFrame fluid stem. First, a 6-second 2D turbo-spin echo was acquired through the distal fluid stem in an orientation perpendicular to the desired trajectory. The scan was acquired at 1 mm in-plane resolution over a 128-mm FOV with a single 10-mm thick slice, a TE of 41 ms, TR of 704 ms, 2 repetitions, an echo train length of 37 and a bandwidth of 400 Hz/pixel. The software used this image to compare the current SmartFrame trajectory to the target trajectory in order to calculate an expected error for tip placement and generate instructions to adjust SmartFrame alignment via the pitch and roll (fig. 3b, c). After these adjustments had been made, the scan was reacquired to measure the new expected error and this process was repeated if necessary.

When the expected error fell <1.0 mm, the pitch and roll axes on the SmartFrame were locked and a 26-second 2D turbo-spin echo scan was acquired along the sagittal and coronal planes of the guide stem for fine adjustment of the SmartFrame X-Y stage. Seven slices of 1 mm isotropic resolution were acquired over a 180 × 240 mm FOV with a TE of 22 ms, a TR of 500 ms, 2 repetitions, an echo train length of 7 and a bandwidth 250 of Hz/pixel. The ClearPoint software used these images to generate instructions for fine adjustment of the trajectory, achieved by dialing-in distance changes on the SmartFrame X-Y stage. This process was repeated until the software reported an expected error of <0.5 mm, which typically required no more than 2 iterations (fig. 3d, e).

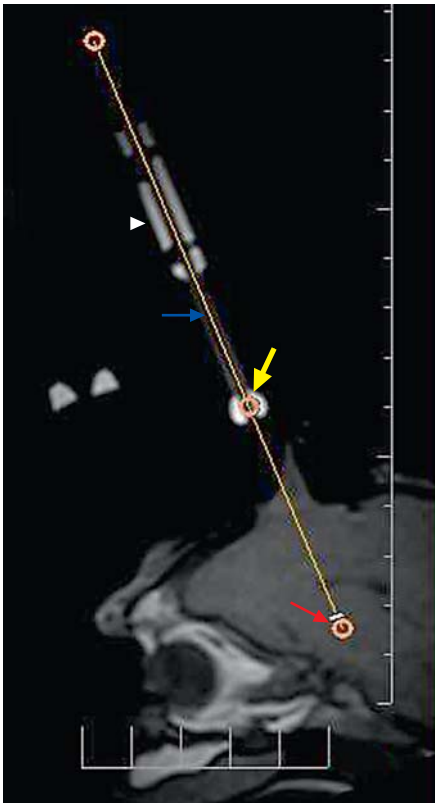

Color version available online

Fig. 2. Sagittal screenshot of target trajectory alignment. The T1 MRI-visible fluid stem (arrowhead), which will hold the infusion cannula, has been aligned by translating the SmartFrame around a fixed pivot point (thick arrow) so that the trajectory (thin arrow) meets the target (red arrow, black in the printed version).

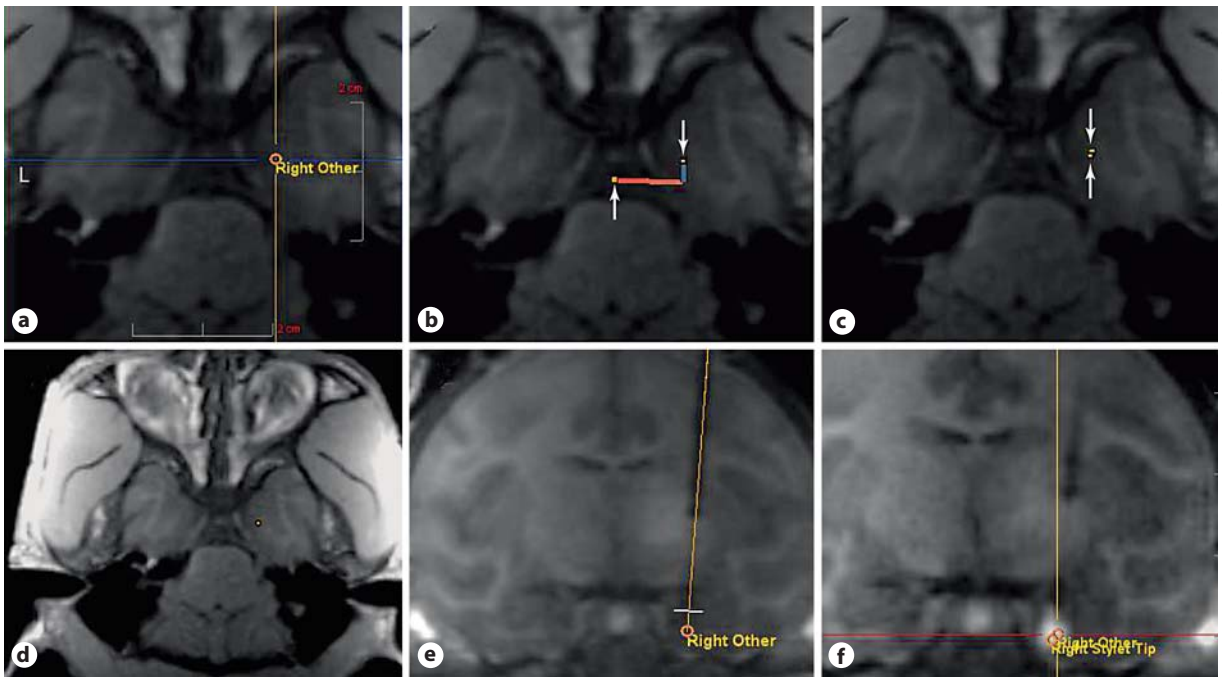

Color version available online

Fig. 3. Sequence for target trajectory alignment using ClearPoint software. **a** The selected target. **b** Pitch (orange/horizontal) and roll (blue/vertical) distances required for proper fluid stem alignment. Note that actual instructions for dialing-in these distances on the handheld controller are reported in a separate panel on the workstation. **c** The predicted error after pitch and roll adjustment, with the small distances remaining corrected by alignment in the X and Y planes. **d** Overlapping of the points indicated by arrows in **b** and **c**, indicating that the current trajectory matches the expected target trajectory. This trajectory is shown in the coronal plane in **e** and again following the infusion in **f**.

The infusion system included a custom-designed, ceramic, fused silica reflux-resistant cannula that was designed in accordance with previously reported principles developed in our laboratory [10, 15]. The cannula dimensions are shown in figure 4. For infusions, the cannula was connected to a loading line containing 1 mM gadoteridol, and the flow was regulated with a trypan-blue-filled, 1-ml syringe mounted onto an MRI-compatible infusion pump (Harvard Bioscience Company). With the aiming device aligned in its final position, the software reported the expected distance from the target to the top of the guide stem, and this distance was measured from the cannula tip and marked on the cannula using a sterile ink marker. A depth stop was then secured at the marked location and the measured insertion distance was verified. The infusion pump was started at 1 μl/min, and after visualizing fluid flow from the cannula tip when held at the height of the bore, the cannula was inserted through the SmartFrame guide stem and into the brain. When the depth stop encountered the top of the guide stem, it was secured with a locking screw.

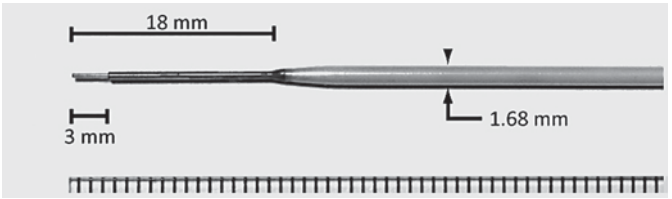

Fig. 4. Custom-designed infusion cannula. The distance between hash marks is 1 mm.

Infusion and Imaging

Following cannula insertion, repeated multiplanar Fast Low Angle Shot (FLASH) images were obtained every 5 min throughout the duration of the infusion. The FLASH images were acquired at an in-plane resolution of 0.7 × 0.7 × 1 mm with 128 slices over the 180-mm FOV at a TE of 4.49 ms, a TR of 17 ms with 2 repetitions and a bandwidth of 160 Hz/pixel. The first scan was acquired with a 4-degree flip angle to produce a proton-density-weighted image for visualization of the cannula tip. All subsequent scans were acquired with a 40-degree flip angle to increase the T1-weighting and highlight the signal enhancement from gadoteridol in the infusate.

Upon visualization of gadoteridol infusion at the cannula tip, the infusion rates were increased from an initial rate of 1 μl/min in a ramping fashion, 0.5 μl/min every 5 min, to reach a maximum of 3 μl/min. The interface between trypan blue and gadoteridol within the loading line was also marked at the start and finish of the infusion in order to verify that the infused volume matched that reported by the pump. Each NHP first received a

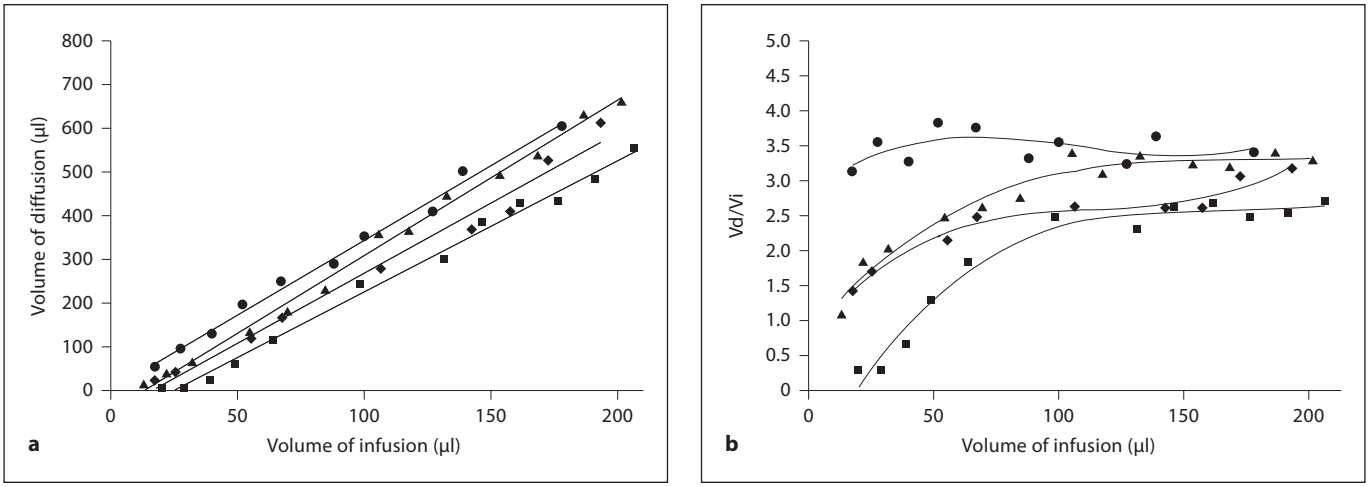

Fig. 5. Vd/Vi relationships. **a** Dependence of Vd on Vi for each individual infusion, with corresponding best-fit linear regression lines. **b** Variation of Vd/Vi with increasing infusion volumes, and corresponding best-fit third-order polynomial trend lines. ● = Infusion 2; ▲ = infusion 5; ■ = infusion 8; ◆ = infusion 11.

small volume infusion in the subthalamic area (16–25 μl) to allow calculation of targeting error, followed by a larger volume infusion (187–230 μl) into the ipsilateral thalamus. In 3 of the infusion sessions, NHP received an additional, smaller volume infusion (17–40 μl) into the substantia nigra (n = 1) or hippocampus (n = 2) to generate further data points for target error calculation. In general, the total time under general anesthesia for NHPs who received 4 sequential infusions was approximately 6 h.

Imaging Data Analysis

Images obtained during RCD were transferred to the ClearPoint system for analysis of targeting error. With the target position hidden from view, the location of the cannula tip was manually selected in the ClearPoint console by identifying the center of the gadoteridol signal in the lower one third of the infusion volume on the first scan demonstrating convection following cannula insertion (fig. 3f). The software then automatically reported the vector distance between the target site and the actual position of the cannula tip. The average target error for all infusions was later calculated and the 95% confidence interval was determined. Spearman's rank-order correlation was used as a nonparametric measure of the statistical dependence between depth to target and target error.

Images obtained during RCD were transferred to a PACS and accessed by Osirix, an open-source DICOM reader and imaging workstation. Distribution volumes and spatial patterns were analyzed using OsiriX software. Regions of interest (ROIs) were manually traced and 3-dimensional volumetric reconstructions were then generated from these ROIs and used to calculate volume of distribution/volume of infusion (Vd/Vi) ratios.

Tissue Processing

Each NHP was perfused transcardially 7 days following its second infusion session. Brains were harvested, sliced in 6-mm coronal sections in a brain matrix, postfixed in 4% paraformaldehyde/PBS and cryoprotected in 30% sucrose. A sliding microtome was used to cut 40-μm serial sections for histological processing. For hematoxylin and eosin (HE) staining, free-floating sections were rehydrated and stained with hematoxylin for 15 s, washed with tap water and then differentiated in 0.5% glacial acetic acid/70% alcohol followed by staining in bluing solution. After incubation in eosin, the sections were dehydrated in alcohol and xylene. For glial fibrillary acid protein (GFAP) and Iba1 immunohistochemistry, the sections were first washed 3 times in PBS for 5 min each followed by treatment with 1% H_2O_2 in PBS for 20 min at room temperature. The sections were then incubated in Sniper blocking solution (Biocare Medical) for 30 min at room temperature followed by incubation with primary antibodies [Iba1, diluted 1:1,000 (Biocare Medical); GFAP, diluted 1:15,000 (Chemicon)] in Da Vinci diluent (Biocare Medical) overnight at room temperature. After 3 rinses in PBS for 5 min each at room temperature, the sections were incubated in Mach 2 horseradish peroxidase polymer (Biocare Medical) for 1 h at room temperature, followed by several washes and colorimetric development with 3,30-diaminobenzidine. Immunostained sections were mounted on slides and sealed with Cytoseal (Richard-Allan Scientific).

Results

Eleven total insertions of the infusion cannula were made, in groups of 2 or 3 different targeting trajectories in 1 hemisphere per infusion session. Satisfactory cannula placement was achieved on the first attempt (without the need for repositioning) in all cases. No technical limitations were encountered in redirecting the cannula for infusing multiple targets in the same hemisphere, which is a novel attribute of this system.

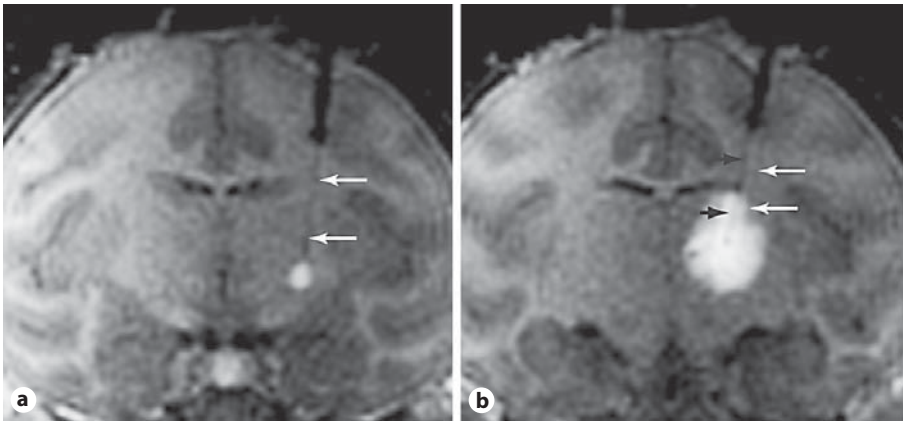

Fig. 6. Adjacent cannula trajectories in a single region. **a** An initial cannula trajectory (white arrows) and infusion in the subthalamic area. **b** The trajectory of the repositioned cannula (black arrows) and a large infusion in the thalamus that has encompassed the previous insertion tract (also visible in this plane, white arrows). No backflow through the initial insertion site is present.

Table 1. Results

Infusion number	Anatomic target	Depth to target, mm	Volume infused, μl	Target error, mm
1	ST	22	16	1.1
2	thalamus	24	187	0.8
3	SN	31	21	0.6
4	ST	27	17	1.0
5	thalamus	25	210	0.8
6	hippocampus	40	40	1.0
7	ST	24	25	0.8
8	thalamus	24	230	0.8
9	hippocampus	34	35	0.5
10	ST	28	18	0.5
11	thalamus	26	205	0.3

Average target error = 0.8 (95% CI = 0.14). ST = Subthalamic area; SN = substantia nigra.

Targeting Accuracy

Each of the anatomic structures chosen for RCD, listed in table 1, was successfully targeted with minimal error. The ClearPoint system automatically calculated each targeting error, defined as the 3-dimensional distance between the expected cannula tip location and the actual location measured on postinsertion imaging. The average targeting error was 0.8 mm (95% CI = 0.1). The target error was independent of the depth of the target from the cortical surface (Spearman rank-order correlation coefficient = –0.34, p = 0.31).

Cannula Performance

No infusions produced cannula occlusion, reflux or distribution beyond the target structure. From the tip of the cannula the Gd-enhanced infusate was observed to immediately spread 3 mm along the cannula, to the step change in fused silica, before distributing in a spherical pattern. In all cases, the infusions proceeded in a predictable fashion to deliver an infusate distribution of contained shape. Larger volume infusions were undertaken in the thalamus in order to evaluate diffusion volume characteristics. Vd was determined from each MRI scan obtained during thalamic infusions and plotted against the Vi for the given time point (fig. 5a). The Vd increased in a predictable, linear fashion as Vi increased in each infusion: the Pearson correlation coefficient for each individual data set ranged from 0.991 to 0.997 (0.968 for the combined data set) and the slope of the linear regression line ranged from 3.0 to 3.6 (average = 3.3, 95% CI = 0.2). Vd/Vi ratios were calculated and plotted as a function of Vi (fig. 5b). The average Vd/Vi at the final infusion volume (range = 178–207 μl) was 3.1 (95% CI = 0.3).

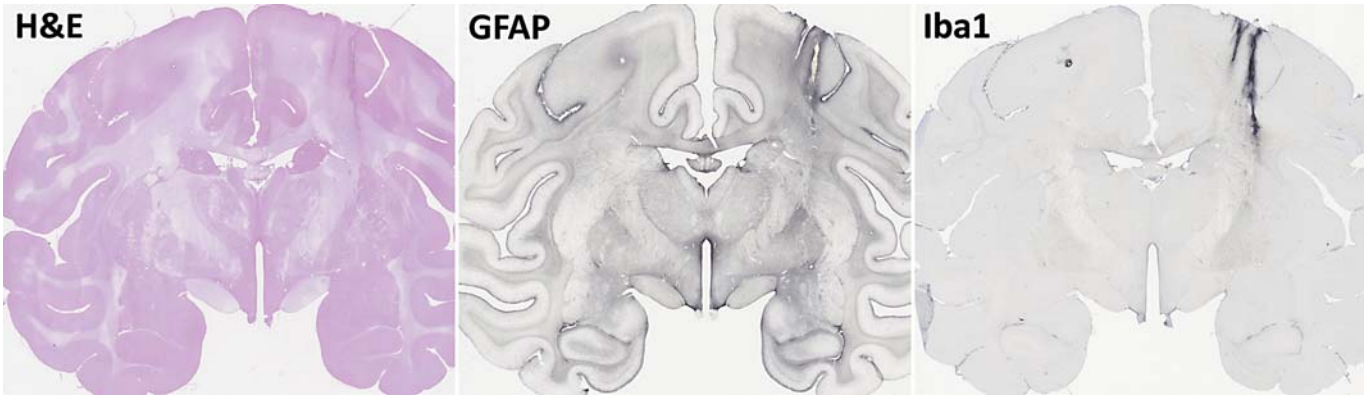

Color version available online

Fig. 7. Lack of tissue damage in subcortical targets. Representative, alternating sections through a plane with 2 cannula tracts demonstrate minimal evidence for tissue damage in the thalamus or hippocampus, which were both targeted on the right side in this animal.

We demonstrated that this system could place 2 infusions in close proximity without producing reflux in the initial cannula tract during the course of the second infusion. Each of the thalamic infusions (178–206 μl) was the second in the infusion series for a given hemisphere and was carried out at a distance of 5–6 mm from the immediately preceding cannula tract that targeted the subthalamic area in each case. In all cases the second, large infusion volume expanded to cover the site of the previous infusion without evidence for reflux into the previous tract (fig. 6).

Cannula Safety

No MRI-visible hemorrhages occurred during cannula placement, and no adverse events occurred during RCD. Standard postoperative care assessments indicated that no RCD-related side effects were observed over the course of these experiments (2 months). Following the final infusion, NHP recovered 7 days before the brains were harvested for assessment of tissue damage by HE staining and GFAP or Iba1 immunohistochemistry. Iba1 is a calcium-binding protein that is specifically expressed in microglia in the brain and is upregulated during the activation of these cells due to inflammation [16]. In each animal, moderate Iba1 and GFAP expression was noted along the cannula tracts but not at the depth of the proximal, fused silica tip (fig. 7), consistent with previous reports demonstrating minimal inflammation following CED from step-designed catheters [17]. HE staining showed no evidence of overt pathology, such as cerebritis, infarcts or cellular infiltrates around the delivery sites.

Discussion

In this study, we described our use of inMRI to perform RCD with submillimetric accuracy in the NHP brain, using a novel skull-mounted aiming device and interactive software system. This platform is based on the concept of prospective stereotaxy, the alignment of a skull-mounted trajectory guide within an MRI system [18], which has been applied in clinical studies to perform brain biopsies [19, 20] and placement of DBS leads [20–22]. The recent development of a clinical program at the University of California San Francisco for placing DBS electrodes by prospective stereotaxy using high-field inMRI was motivated by potential errors inherent to traditional stereotaxy: preoperative image distortion, brain shift occurring after imaging but before brain insertion, and errors arising from the mechanical properties of the frame and guidance system [22]. Regarding the use of traditional stereotaxy for CED, in addition to the above limitations, the inability to visualize infusion progress or complications during drug delivery has necessitated the development of RCD. Application of the ClearPoint system for inMRI-guided direct delivery of therapeutics in the brain is an extension of these efforts.

The goal in developing the RCD platform described here is to facilitate clinical translation of positive results from preclinical intracerebral drug delivery studies. Negative results were reported following the phase I/II non-CED infusion of CERE-120 in Parkinson's patients (AAV2-neurturin) [23]. We believe the failure of neurturin to benefit patients was largely due to inadequate vector delivery (only 15% of putamen covered [24]), given

extensive preclinical evidence that widespread GDNF (a structural and functional analogue of neurturin) expression in the putamen produced significant behavioral improvement in Parkinsonian NHP when AAV2-GDNF is delivered via CED [17, 25, 26]. Likewise, an extensive analysis [27] of the different infusion techniques used in the clinical GDNF infusion studies highlighted the role of variable catheter placement in outcome discrepancies between a randomized controlled study of chronic intraputamenal GDNF protein infusion that did not reach efficacy endpoints [28] and positive results from 2 prior open-label studies [29, 30]. Results from clinical trials employing CED to delivery immunotoxins [31] and chemotherapeutics [32] in brain tumor patients have also demonstrated that poor drug distribution has the potential to cause failure of these clinical studies independent of the efficacy of the therapeutic agent [33].

Targeting Accuracy

The targeting accuracy of this system, calculated as the average vector distance between the expected cannula tip location and the actual location measured using intraoperative imaging, is on the order of <1 mm. Note that, given the slice thickness (1 mm) and voxel dimensions of the targeting scan (0.7 × 0.7 × 1 mm), and subsequent image reconstruction by the ClearPoint system, the actual error of this system is likely within the limits of resolution of the imaging system. The system therefore appears to be highly accurate, and since the targeting error was independent of the target depth (up to distances of 4 cm), achieving a similar target error may be possible for longer trajectories in the human brain. This targeting error compares favorably to both the vector targeting error for DBS lead tip locations reported in a statistical comparison of frame-based and frameless traditional stereotactic techniques (3.2 mm) [34] and to that reported for the recent series of inMRI DBS lead placements by prospective stereotaxy at the University of California San Francisco using a different system, the Medtronic NexFrame (2.2 mm) [22].

This accuracy also surpasses that of our previous experience using RCD in NHP, in protocols where either a guide cannula or a multiport guide array was placed stereotactically with regard to a baseline MRI, prior to the inMRI procedure. Infusion data obtained by these methods were analyzed recently to determine the optimal zones for cannula placement within the putamen, thalamus and brainstem [35, 36] that predict contained distribution within the target region. Images obtained during RCD in those studies showed that distribution of gadolinium tracer outside of the target structure occurred in 64% of putamenal infusions and in 43% of thalamic infusions, clearly demonstrating the need for prospective stereotaxy. In the current study, no infusions in the thalamus produced significant extrathalamic distribution into white matter tracks or leakage into the CSF space due to poor cannula placement. In fact, the accuracy of this system guarantees insertion of the infusion cannula at preselected coordinates within a 'green zone' for optimal distribution within target structures, as we have defined for the NHP putamen, thalamus and brainstem [35]. For instance, in the planning stages, the system allows the user to determine whether the location of the cannula step will fall at least 3 mm from the boundaries of the putamen or thalamus, the general minimal distance required to achieve >98% containment of Gd within these target structures in the studies cited above.

Cannula Performance and Safety

Infusions in the thalamus were used to evaluate cannula distribution properties. In our experience, the NHP putamen and other nuclei smaller than the thalamus are inappropriate targets for testing infusion volumes beyond ~50 μl, due to leakage beyond the anatomic boundaries of these small targets. The distribution properties for clinically relevant volumes (≥50 μl) in grey matter therefore were calculated only from thalamic infusions in this study. We found that the Vd increased in a correlated fashion with increasing Vi, with an average linear slope of 3.3. The corresponding average Vd/Vi at the final infusion volume was 3.1, but as figure 5b demonstrates the measured ratio at any given Vi was not predictive of the final Vd/Vi until ~100 μl had been infused, i.e. Vd/Vi increased during the initial stages of the infusion before reaching a relative plateau. We suspect that early inconsistencies in Vd/Vi reflect variability in tissue dynamics at the cannula tip that equilibrates as the infusion proceeds, after the maximal flow rate has been achieved.

The Vd/Vi relationship is important in RCD for planning drug delivery dosages, as several groups have previously demonstrated the use of an MRI tracer to estimate the Vd of coinfused therapeutic agents, including radiolabeled muscimol [37], GDNF protein [12], AAV viral capsids [38] and AAV2 vector transgene products (in press). In the current study, infusate did not distribute beyond the anatomic boundaries of the thalamus, in contrast to our previous studies and those of others cited above, where extratarget distribution occurred. This important difference may explain the lower Vd/Vi ratio reported here in comparison to the previously reported

ranges of 4–8, as it more closely approximates the Vd/Vi of 3.8 we recently found for gadoteridol infusions that were contained within the NHP thalamus [36].

In addition to the ability to choose the target and trajectory in real time, there are other advantages to the ClearPoint system that may explain improved performance over previous experimental studies. Our laboratory has previously shown that a smaller internal diameter permits a higher reflux-free flow rate with a step-design cannula, which is important for minimizing the infusion time during clinical CED protocols [15]. The dimensions of the 3-mm fused silica tip used here balance well the need for infusate delivery at a high flow rate and physical stability, as qualitatively these infusions appeared to proceed in a more uniform and reproducible fashion than we have previously observed. In comparison to the cannula used in our most recent NHP studies [35], the internal diameter of the current cannula is smaller (200 vs. 324 μm). Additionally, the skull-mounted SmartFrame provides a rigid housing for the cannula that restricts axial movement during brain insertion. This element is especially important in the performance of CED, where small movements at the cannula tip can create tissue disruption leading to reflux of infusate. Taken together, these improvements in cannula design have resulted in infusions of more predictable and reliable quality, although we have not made any direct quantitative comparisons to prior infusions regarding the progressive morphology of infusion volumes.

With respect to other potential safety issues, there were no behavioral or histological indications of parenchymal injury due to cannula insertion, despite multiple cannula placements occurring in each hemisphere of both animals. Given that the diameter of this customized ceramic cannula is only slightly larger than that of a standard DBS lead (1.67 vs. 1.27 mm, respectively), it appears to be quite safe. Studies are ongoing to generate IND-level cannula safety data.

Future Development

The ability of this platform to deliver controlled volumes of drug to any structure in the NHP brain with accuracy on the order of 1 mm and the capacity to monitor the infusion in real time expands opportunities for using the NHP brain to model human disease and therapies. The NHP brain is uniquely suited for neurosurgical experimental investigation, due to similarities between human and primate anatomy and physiology that cannot be modeled in other species [39]. We anticipate that the system described here will facilitate the creation of new NHP disease models due to a novel ability for precise viral vector infusion and subsequent transgene expression in discrete brain regions. In addition, we expect that ongoing studies will allow modeling of specific patterns of viral vector distribution and subsequent gene expression in structures to be targeted using this system in clinical trials, e.g. mapping infusions in the putamen for Parkinson's disease. These ongoing studies also seek to define the expected in-magnet time required for these clinical procedures.

The evolution of this system also is envisioned to include tools that aid the neurosurgeon in planning, delivering and anticipating the functional outcome of infusions into multiple brain locations. For instance, initiatives to incorporate the autosegmentation of target structures and surrounding anatomy, as well as autosegmentation of infusion volumes in real time, are underway. Eventually, analysis of retrospective and prospective infusion data in the NHP brain should allow the development of predictive algorithms that will ultimately allow the system software to forecast areas of drug distribution or transgene expression based on a selected location for cannula tip placement.

Conclusion

The ClearPoint system allows RCD to be performed with a high level of precision, predictability and safety. This technique should increase the utility of RCD for producing new NHP disease models and will expand the scope of preclinical drug delivery studies. Clinical application of this platform is likely to improve the success rate for clinical trials employing intracerebral drug delivery by direct infusion.

Acknowledgment

The study was supported by NIH grant P01 CA118816 to K.S.B. and F32 NS064692 to R.M.R.

Disclosure Statement

P.P., G.B. and L.T. are employees of SurgiVision, Inc., which produces the ClearPoint device.

References

1 Bobo RH, Laske DW, Akbasak A, Morrison PF, Dedrick RL, Oldfield EH: Convection-enhanced delivery of macromolecules in the brain. Proc Natl Acad Sci USA 1994;91:2076–2080.

2 Bankiewicz KS, Eberling JL, Kohutnicka M, Jagust W, Pivirotto P, Bringas J, Cunningham J, Budinger TF, Harvey-White J: Convection-enhanced delivery of AAV vector in parkinsonian monkeys; in vivo detection of gene expression and restoration of dopaminergic function using pro-drug approach. Exp Neurol 2000;164:2–14.

3 Bankiewicz KS, Forsayeth J, Eberling JL, Sanchez-Pernaute R, Pivirotto P, Bringas J, Herscovitch P, Carson RE, Eckelman W, Reutter B, Cunningham J: Long-term clinical improvement in MPTP-lesioned primates after gene therapy with AAV-HAADC. Mol Ther 2006;14:564–570.

4 Daadi MM, Pivirotto P, Bringas J, Cunningham J, Forsayeth J, Eberling J, Bankiewicz KS: Distribution of AAV2-HAADC-transduced cells after 3 years in parkinsonian monkeys. Neuroreport 2006;17:201–204.

5 Forsayeth JR, Eberling JL, Sanftner LM, Zhen Z, Pivirotto P, Bringas J, Cunningham J, Bankiewicz KS: A dose-ranging study of AAV-HAADC therapy in parkinsonian monkeys. Mol Ther 2006;14:571–577.

6 Christine CW, Starr PA, Larson PS, Eberling JL, Jagust WJ, Hawkins RA, VanBrocklin HF, Wright JF, Bankiewicz KS, Aminoff MJ: Safety and tolerability of putaminal AADC gene therapy for parkinson disease. Neurology 2009;73:1662–1669.

7 Eberling JL, Jagust WJ, Christine CW, Starr P, Larson P, Bankiewicz KS, Aminoff MJ: Results from a phase I safety trial of HAADC gene therapy for parkinson disease. Neurology 2008;70:1980–1983.

8 Nguyen TT, Pannu YS, Sung C, Dedrick RL, Walbridge S, Brechbiel MW, Garmestani K, Beitzel M, Yordanov AT, Oldfield EH: Convective distribution of macromolecules in the primate brain demonstrated using computerized tomography and magnetic resonance imaging. J Neurosurg 2003;98:584–590.

9 Richardson RM, Varenika V, Forsayeth JR, Bankiewicz KS: Future applications: gene therapy. Neurosurg Clin N Am 2009;20:205–210.

10 Fiandaca MS, Forsayeth JR, Dickinson PJ, Bankiewicz KS: Image-guided convection-enhanced delivery platform in the treatment of neurological diseases. Neurotherapeutics 2008;5:123–127.

11 Fiandaca MS, Varenika V, Eberling J, McKnight T, Bringas J, Pivirotto P, Beyer J, Hadaczek P, Bowers W, Park J, Federoff H, Forsayeth J, Bankiewicz KS: Real-time MR imaging of adeno-associated viral vector delivery to the primate brain. Neuroimage 2009;47(suppl 2):T27–T35.

12 Gimenez F, Krauze MT, Valles F, Hadaczek P, Bringas J, Sharama N, Forsayeth J, Bankiewicz KS: Image-guided convection-enhanced delivery of GDNF protein into monkey putamen. Neuroimage 2011;54(suppl 1):S189–195.

13 Su X, Kells AP, Aguilar Salegio EA, Richardson RM, Hadaczek P, Beyer J, Bringas J, Pivirotto P, Forsayeth J, Bankiewicz KS: Real-time MR imaging with gadoteridol predicts distribution of transgenes after convection-enhanced delivery of AAV2 vectors. Mol Ther 2010;18:1490–1495.

14 Lonser RR, Warren KE, Butman JA, Quezado Z, Robison RA, Walbridge S, Schiffman R, Merrill M, Walker ML, Park DM, Croteau D, Brady RO, Oldfield EH: Real-time image-guided direct convective perfusion of intrinsic brainstem lesions. Technical note. J Neurosurg 2007;107:190–197.

15 Krauze MT, Saito R, Noble C, Tamas M, Bringas J, Park JW, Berger MS, Bankiewicz K: Reflux-free cannula for convection-enhanced high-speed delivery of therapeutic agents. J Neurosurg 2005;103:923–929.

16 Ito D, Imai Y, Ohsawa K, Nakajima K, Fukuuchi Y, Kohsaka S: Microglia-specific localisation of a novel calcium binding protein, Iba1. Brain Res Mol Brain Res 1998;57:1–9.

17 Su X, Kells AP, Huang EJ, Lee HS, Hadaczek P, Beyer J, Bringas J, Pivirotto P, Penticuff J, Eberling J, Federoff HJ, Forsayeth J, Bankiewicz KS: Safety evaluation of AAV2-GDNF gene transfer into the dopaminergic nigrostriatal pathway in aged and parkinsonian rhesus monkeys. Hum Gene Ther 2009;20:1627–1640.

18 Truwit CL, Liu H: Prospective stereotaxy: a novel method of trajectory alignment using real-time image guidance. J Magn Reson Imaging 2001;13:452–457.

19 Hall WA, Liu H, Martin AJ, Maxwell RE, Truwit CL: Brain biopsy sampling by using prospective stereotaxis and a trajectory guide. J Neurosurg 2001;94:67–71.

20 Martin AJ, Hall WA, Roark C, Starr PA, Larson PS, Truwit CL: Minimally invasive precision brain access using prospective stereotaxy and a trajectory guide. J Magn Reson Imaging 2008;27:737–743.

21 Martin AJ, Larson PS, Ostrem JL, Keith Sootsman W, Talke P, Weber OM, Levesque N, Myers J, Starr PA: Placement of deep brain stimulator electrodes using real-time high-field interventional magnetic resonance imaging. Magn Reson Med 2005;54:1107–1114.

22 Starr PA, Martin AJ, Ostrem JL, Talke P, Levesque N, Larson PS: Subthalamic nucleus deep brain stimulator placement using high-field interventional magnetic resonance imaging and a skull-mounted aiming device: technique and application accuracy. J Neurosurg 2010;112:479–490.

23 Marks WJ Jr, Bartus RT, Siffert J, Davis CS, Lozano A, Boulis N, Vitek J, Stacy M, Turner D, Verhagen L, Bakay R, Watts R, Guthrie B, Jankovic J, Simpson R, Tagliati M, Alterman R, Stern M, Baltuch G, Starr PA, Larson PS, Ostrem JL, Nutt J, Kieburtz K, Kordower JH, Olanow CW: Gene delivery of AAV2-neurturin for parkinson's disease: a double-blind, randomised, controlled trial. Lancet Neurol 2010;9:1164–1172.

24 Bartus RT, Herzog CD, Chu Y, Wilson A, Brown L, Siffert J, Johnson EM Jr, Olanow CW, Mufson EJ, Kordower JH: Bioactivity of AAV2-neurturin gene therapy (CERE-120): differences between Parkinson's disease and nonhuman primate brains. Mov Disord 2010, Epub ahead of print.

25 Eberling JL, Kells AP, Pivirotto P, Beyer J, Bringas J, Federoff HJ, Forsayeth J, Bankiewicz KS: Functional effects of AAV2-GDNF on the dopaminergic nigrostriatal pathway in parkinsonian rhesus monkeys. Hum Gene Ther 2009;20:511–518.

26 Johnston LC, Eberling J, Pivirotto P, Hadaczek P, Federoff HJ, Forsayeth J, Bankiewicz KS: Clinically relevant effects of convection-enhanced delivery of AAV2-GDNF on the dopaminergic nigrostriatal pathway in aged rhesus monkeys. Hum Gene Ther 2009;20:497–510.

27 Morrison PF, Lonser RR, Oldfield EH: Convective delivery of glial cell line-derived neurotrophic factor in the human putamen. J Neurosurg 2007;107:74–83.

28 Lang AE, Gill S, Patel NK, Lozano A, Nutt JG, Penn R, Brooks DJ, Hotton G, Moro E, Heywood P, Brodsky MA, Burchiel K, Kelly P, Dalvi A, Scott B, Stacy M, Turner D, Wooten VG, Elias WJ, Laws ER, Dhawan V, Stoessl AJ, Matcham J, Coffey RJ, Traub M: Randomized controlled trial of intraputamenal glial cell line-derived neurotrophic factor infusion in Parkinson disease. Ann Neurol 2006;59:459–466.

29 Patel NK, Bunnage M, Plaha P, Svendsen CN, Heywood P, Gill SS: Intraputamenal infusion of glial cell line-derived neurotrophic factor in PD: a two-year outcome study. Ann Neurol 2005;57:298–302.

30 Slevin JT, Gerhardt GA, Smith CD, Gash DM, Kryscio R, Young B: Improvement of bilateral motor functions in patients with Parkinson disease through the unilateral intraputaminal infusion of glial cell line-derived neurotrophic factor. J Neurosurg 2005;102:216–222.

31 Sampson JH, Archer G, Pedain C, Wembacher-Schroder E, Westphal M, Kunwar S, Vogelbaum MA, Coan A, Herndon JE, Raghavan R, Brady ML, Reardon DA, Friedman AH, Friedman HS, Rodriguez-Ponce MI, Chang SM, Mittermeyer S, Croteau D, Puri RK: Poor drug distribution as a possible explanation for the results of the PRECISE trial. J Neurosurg 2010;13:301–309.

32 Lidar Z, Mardor Y, Jonas T, Pfeffer R, Faibel M, Nass D, Hadani M, Ram Z: Convection-enhanced delivery of paclitaxel for the treatment of recurrent malignant glioma: a phase I/II clinical study. J Neurosurg 2004;100:472–479.
33 Sampson JH, Raghavan R, Provenzale JM, Croteau D, Reardon DA, Coleman RE, Rodriguez Ponce I, Pastan I, Puri RK, Pedain C: Induction of hyperintense signal on T2-weighted MR images correlates with infusion distribution from intracerebral convection-enhanced delivery of a tumor-targeted cytotoxin. AJR Am J Roentgenol 2007;188:703–709.
34 Holloway KL, Gaede SE, Starr PA, Rosenow JM, Ramakrishnan V, Henderson JM: Frameless stereotaxy using bone fiducial markers for deep brain stimulation. J Neurosurg 2005;103:404–413.
35 Yin D, Valles FE, Fiandaca MS, Bringas J, Gimenez F, Berger MS, Forsayeth J, Bankiewicz KS: Optimal region of the putamen for image-guided convection-enhanced delivery of therapeutics in human and non-human primates. Neuroimage 2009, Epub ahead of print.
36 Yin D, Richardson RM, Fiandaca MS, Bringas J, Forsayeth J, Berger MS, Bankiewicz KS: Cannula placement for effective convection-enhanced delivery in the nonhuman primate thalamus and brainstem: implications for clinical delivery of therapeutics. J Neurosurg 2010;113:240–248.
37 Heiss JD, Walbridge S, Asthagiri AR, Lonser RR: Image-guided convection-enhanced delivery of muscimol to the primate brain. J Neurosurg 2010;112:790–795.
38 Szerlip NJ, Walbridge S, Yang L, Morrison PF, Degen JW, Jarrell ST, Kouri J, Kerr PB, Kotin R, Oldfield EH, Lonser RR: Real-time imaging of convection-enhanced delivery of viruses and virus-sized particles. J Neurosurg 2007;107:560–567.
39 Richardson RM, Larson PS, Bankiewicz KS: Gene and cell delivery to the degenerated striatum: status of preclinical efforts in primate models. Neurosurgery 2008;63:629–642; discussion 642–644.